Transportation Research Part C 89 (2018) 364–383

Contents lists available at ScienceDirect

Transportation Research Part C

journal homepage: www.elsevier.com/locate/trc

Spatiotemporal intersection control in a connected and automated vehicle environment

Yiheng Feng[a], Chunhui Yu[b,c], Henry X. Liu[a,c,*]

[a] University of Michigan Transportation Research Institute (UMTRI), University of Michigan, Ann Arbor, United States
[b] Key Laboratory of Road and Traffic Engineering of the Ministry of Education, Tongji University, China
[c] Department of Civil and Environmental Engineering, University of Michigan, Ann Arbor, United States

ARTICLE INFO

Keywords:
Connected and automated vehicle
Traffic signal control
Vehicle trajectory control
Delay and emission reduction

ABSTRACT

Current research on traffic control has focused on the optimization of either traffic signals or vehicle trajectories. With the rapid development of connected and automated vehicle (CAV) technologies, vehicles equipped with dedicated short-range communications (DSRC) can communicate not only with other CAVs but also with infrastructure. Joint control of vehicle trajectories and traffic signals becomes feasible and may achieve greater benefits regarding system efficiency and environmental sustainability. Traffic control framework is expected to be extended from one dimension (either spatial or temporal) to two dimensions (spatiotemporal). This paper investigates a joint control framework for isolated intersections. The control framework is modeled as a two-stage optimization problem with signal optimization at the first stage and vehicle trajectory control at the second stage. The signal optimization is modeled as a dynamic programming (DP) problem with the objective to minimize vehicle delay. Optimal control theory is applied to the vehicle trajectory control problem with the objective to minimize fuel consumption and emissions. A simplified objective function is adopted to get analytical solutions to the optimal control problem so that the two-stage model is solved efficiently. Simulation results show that the proposed joint control framework is able to reduce both vehicle delay and emissions under a variety of demand levels compared to fixed-time and adaptive signal control when vehicle trajectories are not optimized. The reduced vehicle delay and CO_2 emissions can be as much as 24.0% and 13.8%, respectively for a simple two-phase intersection. Sensitivity analysis suggests that maximum acceleration and deceleration rates have a significant impact on the performance regarding both vehicle delay and emission reduction. Further extension to a full eight-phase intersection shows a similar pattern of delay and emission reduction by the joint control framework.

1. Introduction

Current traffic signal control strategies, including fixed-time, vehicle-actuated and adaptive control, allocate green times to different vehicle movements to avoid conflicts at intersections. Infrastructure-based vehicle detection systems are widely used to collect real-time traffic data as the input to control algorithms. With the rapid development of connected and automated vehicle (CAV) technologies, vehicles can communicate with roadside equipment (RSE) through dedicated short range communications (DSRC). Data collected at RSE provide much richer information on vehicle states than conventional detector data. At the same time,

* Corresponding author at: Department of Civil and Environmental Engineering, University of Michigan, Ann Arbor, United States.
E-mail address: henryliu@umich.edu (H.X. Liu).

https://doi.org/10.1016/j.trc.2018.02.001
Received 13 August 2016; Received in revised form 18 January 2018; Accepted 2 February 2018

data from RSE (e.g. signal status and intersection map) can be broadcast to vehicles within the communication range. The two-way real-time communication between CAVs and infrastructure makes vehicles "controllable" through either speed advisory systems in human-driven connected vehicles or control systems in CAVs.

Therefore, in a CAV environment, not only traffic signals but also vehicle trajectories can be controlled to improve traffic efficiency and gain environmental benefits. Control framework is expected to be extended from one dimension (either spatial or temporal) to two dimensions (spatiotemporal). However, current research efforts mainly address only one side of the joint control problem.

Eco-driving and speed advisory mainly focus on vehicle trajectory control, which is spatial control of vehicle movements. These applications assume that signal timing is fixed and known to vehicles. Optimal control or feedback control (Yang and Jin, 2014) models are built. It is often difficult to solve an optimal control model efficiently in case of complex objective or constraint formulations. Therefore, different simplification methods are proposed to address this issue. A typical method is to divide a vehicle trajectory into several segments with constant acceleration/deceleration for each segment (He et al., 2015; Wu et al., 2015). The optimal control problem is transformed into a nonlinear optimization problem with much fewer decision variables. In addition to trajectory segmentation, numerical solution algorithms are often applied. Meta-heuristics such as genetic algorithm, or gradient-based method, for example, offered by General Pseudospectral Optimal Control Software (GPOPS), can be used to solve various optimal control problems (Benson et al., 2006; Garg et al., 2010; Rao et al., 2010). However, this method may be computationally intensive, especially with a large problem size and the solutions may be worse than the approximation model (He et al., 2015). While most of the studies try to address the trajectory control of an individual vehicle or a few vehicles, a parsimonious shooting heuristic (SH) algorithm was proposed to construct all vehicle trajectories considering vehicle kinematic limits, traffic arrival patterns, car-following safety and signal operations (Ma et al., 2016; Zhou et al., 2017).

CAV based signal control applications consider vehicle trajectories as the input to signal control algorithms, which perform temporal control of traffic signals, and vehicle trajectories are not optimized. Real-time trajectory data (e.g., location, speed, and acceleration) of CAVs are used for signal optimization, based on which phase sequences and green durations are optimized. Link parameters such as traffic demand and queue length are calculated for phase skipping, extension or interruption (Gradinescu et al., 2007). Standard North American NEMA dual-ring, eight-phase controller is usually adopted to generate the optimal signal phase sequence and duration (Feng et al., 2015; He et al., 2012). Minimization of vehicle delay is considered as the optimization objective, and the problem is solved using different optimization techniques such as dynamic programming (DP) or mixed integer linear programming (MILP). In addition to using delay in the objective function, other performance metrics are explored such as weighted cumulative waiting time (WCWT) (Datesh et al., 2011) and cumulative travel time (CTT) (Lee et al., 2013). Instead of mathematical optimization models, microscopic simulations are also applied with vehicle trajectory data for optimal signal plans (Goodall et al., 2013).

One notable solution to the joint control problem of vehicle trajectories and traffic signals is so-called "signal free" intersections where traffic signals are removed, and all vehicles pass the intersection in a self-organized way (Lee and Park, 2012; Zohdy and Rakha, 2014). However, this approach requires 100% penetration rate of fully automated vehicles, which is not realistic in the near future. It can be predicted that in the next ten to twenty years, traffic signals will still play an important role in urban transportation operations.

Another related study which investigated the joint control problem (Li et al., 2014) intuitively divided a vehicle trajectory into four segments with constant acceleration and deceleration rates to reduce the number of decision variables. However, no mathematical proofs were given regarding the optimal number of trajectory segments in terms of fuel consumption or emissions under different situations, which are specifically addressed in this paper. The signal control algorithm enumerated all possible timing plans, which cannot be extended to complex phase structures.

This paper proposes an integrated framework for joint control of traffic signals and vehicle trajectories. A two-stage optimization model is built where traffic signals and vehicle trajectories are optimized sequentially. DP is applied to the signal control problem with the objective to minimize vehicle travel time delay. Optimal control theory is applied to control the trajectories of platoon leading vehicles with the objective to minimize fuel consumption and emission. The trajectories of following vehicles are captured by a car-following model. Currently, a fully CAV environment is assumed, where all vehicle are controllable, although only a few vehicles are controlled. To identify the leading vehicle of each platoon, a platoon identification algorithm is designed. A simplified objective function is proposed for the vehicle trajectory control model, and analytical solutions are derived.

The rest of the paper is organized as follows. Section 2 introduces the methodologies of the joint control framework. Section 3 provides the rolling horizon scheme to perform the two-stage optimization. Section 4 presents numerical examples through simulation and sensitivity analysis on critical parameters. Section 5 concludes the paper and lays out the direction of further research.

2. Model formulations

2.1. Notations

Before the model presentation, notations are summarized in Table 1. The notations in brackets represent the same variable with some of the subscripts omitted for simplicity.

Table 1
Variables and notations.

Variables	Meanings
Car-following model	
n	Vehicle index
$x_n(t)$ [$x(t)$]	Location of n^{th} vehicle at time t (m)
$v_n(t)$ [$v(t)$]	Speed of n^{th} vehicle at time t (m/s)
$u_n(t)$ [$u(t)$]	Acceleration/deceleration rate of n^{th} vehicle at time t (m/s^2)
Δt	Simulation step (sec)
τ_n	Reaction time of vehicle n (sec)
l_n	Length of vehicle n (m)
g_n^{jam}	Jam spacing between vehicles n and $n-1$ (m)
a_n^U [a^U]	Maximum acceleration rate of vehicle n (m/s^2)
a_n^L [a^L]	Maximum deceleration rate of vehicle n (m/s^2)
v_n^f [v^f]	Free flow speed of vehicle n (m/s)
Signal optimization	
J	Total number of stages planned in DP
j	Index of stage (phase) in DP
T	Total time in the planning horizon
P	Number of phases in one cycle
p	Phase Index
s_j	State variable denoting the total number of time steps planned up to stage j
x_j	Control variable denoting the number of time steps planned in stage j
$X_j(s_j)$	Set of feasible control variables in stage j given the total time planned s_j
$v_j(s_j)$	Cumulative value function up to stage j given the total time planned s_j
$f_j(s_j, x_j)$	Performance function at stage j, given s_j and x_j
X_j^{min}	Minimum phase time of stage j (sec)
X_j^{max}	Maximum phase time of stage j (sec)
g_{min}	Minimum green time (sec)
g_{max}	Maximum green time (sec)
g_{tran}	Transition interval (yellow plus red-clearance) (sec)
Platoon identification	
g_p	Remaining green time of phase p (sec)
r_p	Remaining red time of phase p (sec)
h_s	Saturation headway (sec)
d_{DSRC}	DSRC range (m)
d_{max}	Furthest distance that a vehicle can be included in the first platoon (m)
Vehicle trajectory control	
t_0	Time point when the trajectory control begins (sec)
t_f	Time point when the vehicle arrives at the intersection (sec)
v_o	Vehicle speed at time t_0 (m/s)
v_{tf}	Vehicle speed at time t_f (m/s)
L	Distance to the intersection at time t_0 (m)
v_{a^L}	Initial vehicle speed with maximum deceleration all the time (m/s)
v_{a^U}	Initial vehicle speed with maximum acceleration all the time (m/s)

2.2. Model framework

The proposed joint control framework aims at improving the efficiency of green time utilization to minimize vehicle delay and smoothing vehicle trajectories to reduce fuel consumption and emissions. Fig. 1 shows the comparison of green time utilization between the state-of-practice signal control and the proposed joint control.

The blue curve shows the vehicle discharging rate at an intersection under current signal control strategies. When signals turn to green, the first few seconds of the green time are wasted (start-up lost time t_{sl}) because of the reaction time of human drivers. Then the discharging rate increases to the saturation flow rate (q_s) until queued vehicles are fully discharged. Finally, it drops to the arrival rate which is usually lower than the saturation flow rate. The area below the curve is the vehicle demand served during the green time. In the proposed framework, the trajectory of the leading vehicle of an approaching platoon is controlled so that it arrives at the intersection at the beginning of the green time with a certain speed. The control of the leading vehicle trajectory also results in a compact platoon so that the discharging rate keeps the saturation flow rate (as shown in the black dashed line). If Area 3 is equal to the summation of Area 1 and Area 2, then within a much shorter green time interval (g_{new}), the same number of vehicles can pass the intersection as in current control strategies where the green time is much longer (g_{cur}). As a result, the green time utilization is greatly improved. Note that the proposed framework does not increase intersection capacity by shortening the saturation headway, but by utilizing green time more efficiently.

To achieve this goal, a two-stage optimization model is proposed. In the first stage, adaptive signal control concept is adopted to

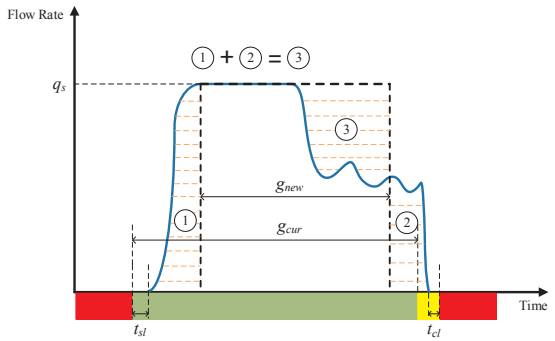

Fig. 1. Green time utilization comparison.

address flow fluctuations. Total vehicle delay is used as the objective function (1):

$$\min_{g_p,u_p} D = \sum D_p(g_p,u_p) = \sum_p \sum_n d_{p,n}(g_p,u_p) \tag{1}$$

$$\text{s.t.} \quad \boldsymbol{g}(g_p,u_p) \leqslant 0 \tag{2}$$

where $d_{p,n}$ is the delay of vehicle n in phase p; g_p is the remaining green time of phase p; u_p is the acceleration/deceleration rate profile of the leading vehicle in phase p. u_p, given the value of g_p, is the solution of the second stage problem. Note that the first-stage optimization does not generate a fixed cycle length, but the cycle length is bounded by the minimum and maximum green times of each phase. Constraint (2) mainly includes signal timing parameters (e.g. minimum and maximum green time) and car-following rules. The detailed formulation of the objective function and constraints of adaptive signal control can be found in Section 2.4.

At the second stage, the trajectory of each leading vehicle is controlled to minimize fuel consumption and emissions in Eq. (3).

$$\min_{u_p} J(g_p,u_p) \tag{3}$$

$$\text{s.t.} \quad \boldsymbol{h}(g_p,u_p) \leqslant 0 \tag{4}$$

As shown in Fig. 2, the objective of the trajectory control is to make the leading vehicle arrive at the intersection (distance L) at time point t_f, which is the beginning of green, with a certain speed v_{tf} (Fig. 2). Constraint (4) presents vehicle dynamics limits (e.g. maximum acceleration), travel time and travel distance. For simplicity, some assumptions are made. All vehicles are homogenous, which have the same size and vehicle dynamics (e.g. acceleration, desired speed). All vehicles are light vehicles and have no time delay on acceleration and deceleration. All following vehicles obey certain car following rules, based on which following vehicles with larger gaps will try to catch up with their leading vehicles with safety constraints. Lane changing and overtaking behaviors are prohibited. Therefore, a compact platoon can be generated naturally without controlling the trajectories of all vehicles.

Signals are the decision variables in the first stage problem. Vehicle trajectories are then optimized in the second stage problem based on the signals at the first stage. With both signals and vehicle trajectory profiles, delay in the first stage problem is calculated.

2.3. Trajectory control

2.3.1. Leading vehicle trajectory control

The trajectories of platoon leading vehicles are controlled to arrive at the intersection at the beginning of green with a certain speed. An optimal control model is formulated:

$$\min_{u(t)} J = \int_{t_0}^{t_f} |u(t)|dt \tag{5}$$

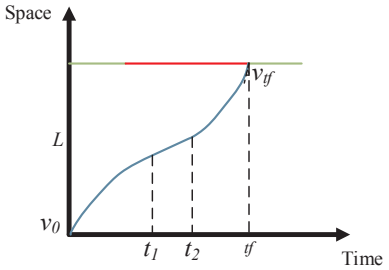

Fig. 2. Leading vehicle trajectory control.

$$\begin{cases} \dot{x}(t) = v(t) \\ \dot{v}(t) = u(t) \end{cases}, t_0 \leqslant t \leqslant t_f \tag{6}$$

$$\begin{cases} x(t_0) = 0 \\ v(t_0) = v_0 \end{cases} \tag{7}$$

$$\begin{cases} x(t_f) = L \\ v(t_f) = v_{tf} \end{cases} \tag{8}$$

$$-a^L \leqslant u(t) \leqslant a^U, \forall\ t_0 \leqslant t \leqslant t_f \tag{9}$$

Vehicle position $x(t)$ and speed $v(t)$ at time t are the state variables. Vehicle acceleration rate $u(t)$ is the control variable and is bounded by maximum deceleration $-a^L$ and acceleration rates a^U as shown in Eq. (9). The relationship between the state variables and the control variable which defines the vehicle dynamics is expressed in Eq. (6). The initial and final states are defined in Eqs. (7) and (8), respectively. $t_0 = 0$ is the time when trajectory control begins. t_f is the departure time of the leading vehicle at the intersection. v_o is the vehicle's current speed. v_{tf} is the vehicle's speed passing the intersection. And L is the distance to the intersection from the current position, which is the total distance traveled by the vehicle. From the formulation, it can be seen that the total travel time and travel distance of the leading vehicle is constrained by Eq. (8). The objective function (5) is used to minimize acceleration and deceleration fluctuations over time in order to reduce fuel consumption or emissions. The purpose of using this simplified formulation is to derive analytical solutions by the *Pontryagin's minimum principle* (PMP) (Sethi and Thompson, 2000), which greatly reduces computational time. The derivation of analytical solutions and proofs of optimality is illustrated in detail in Appendix A. It can be seen from the analysis that the optimal trajectory consists of no more than three segments. As an example, Fig. 3 shows a general optimal trajectory in which the switch time t_1 and t_2 can be obtained uniquely by solving Eqs. (10) and (11) with the constraint of $t_1 < t_2$. For acceleartion trajectory segment, just replace $-a^L$ with a^U.

$$\frac{v_0 + v_c}{2} t_1 + v_c(t_2 - t_1) + \frac{v_{tf} + v_c}{2}(t_f - t_2) = L \tag{10}$$

$$v_c = v_0 - a^L t_1 = v_{tf} + a^L(t_f - t_2) \tag{11}$$

To justify whether the simplified objective function is appropriate, EPA's MOVES emission model (EPA, 2002) is applied as the objective function for comparison as described in detail in Section 2.5.

2.3.2. Platoon identification

To identify the leading vehicle of each platoon to apply the optimal control model, a platoon identification algorithm is developed to separate platoons for different cycles within the DSRC communication range, as shown in Fig. 4. Grey vehicles represent platoon leading vehicles, and black vehicles represent following vehicles. Platoons are identified one by one from the stop-bar. The number of identified platoons is related to the DSRC communication range as well as the number of cycles planned in DP. Generally, the platoon number should be less than or equal to the cycle number planned in DP. In reality, due to the limited range of DSRC communication (e.g. 300 m), usually only one or at most two platoons can be identified for each phase with a reasonable cycle length. The following illustrations are based on only one cycle planned in DP. The analysis is similar if more cycles are planned.

The platoon size for phase p is limited by several factors:

1. The duration of the green time generated by DP in signal optimization. The maximum number of vehicles can be calculated as $floor(g_p/h_s)$, where g_p is the remaining green time of phase p, h_s is the saturation headway, and the *floor* function means rounding down to the next integer.

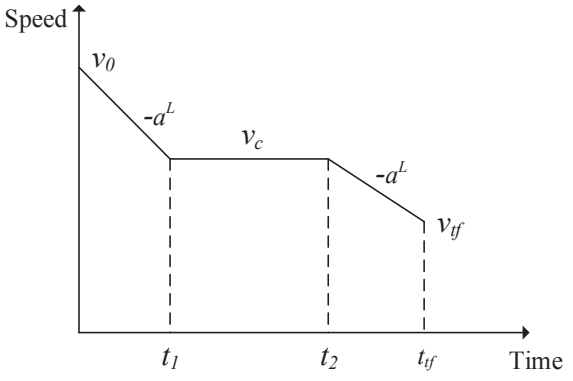

Fig. 3. A general optimal trajectory.

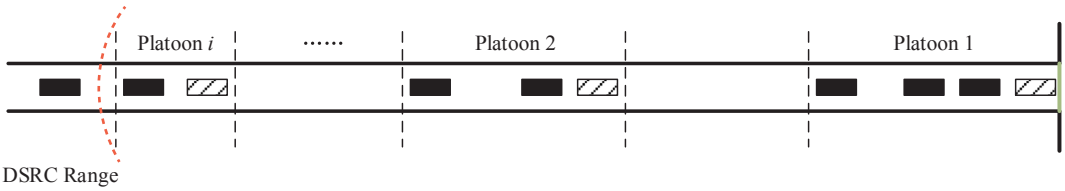

Fig. 4. Platoon identification.

2. Vehicle location. If a vehicle is too far away from the stop-bar, then it may not be able to catch the platoon. The furthest distance d_{max} that a vehicle can be included in the first platoon is calculated as $d_{max} = (r_p + g_p) \times v^f$, where r_p is the remaining red time of phase p and v^f is the free flow speed. If phase p is the current phase, then $r_p = 0$.
3. DSRC range d_{DSRC}. If a vehicle is outside the DSRC range, then it will not be included in the platoon identification algorithm.

In summary, if a vehicle's sequence in the approaching vehicles is less than or equal to $floor(g_p/h_s)$ and its distance to the intersection is small than $\min(d_{max}, d_{DSRC})$, this vehicle can be included in the first platoon. Otherwise, it should be included in other platoons and pass the intersection without stops at stop-bars in later cycles. Therefore, no queues will be generated at stop-bars.

2.3.3. Car-following model

To model the behaviors of following vehicles in a platoon, the Next Generation Simulation (NGSIM) car-following model (Yeo et al., 2008) is adopted to update their trajectories. This car-following model is based on Newell's linear car-following (Newell, 2002) model with additional safety constraints to avoid collisions (Gipps, 1981). The model also considers vehicle performance limits such as maximum acceleration and deceleration rates. The model is described as

$$x_n(t + \Delta t) = \max\{x_n^U(t + \Delta t), x_n^L(t + \Delta t)\} \tag{12}$$

where $x_n(t)$ is the location of n^{th} vehicle at time t; Δt is the simulation step; $x_n^U(t)$ and $x_n^L(t)$ are the upper and lower bounds of $x_n(t)$. The vehicle location at time $t + \Delta t$ is the maximum of an upper bound and a lower bound travel distance.

The upper bound is determined by four factors: car-following rules, acceleration capability, free flow speed and maximum safety distance to avoid collisions. The upper bound travel distance can be expressed as follows:

$$x_n^U(t + \Delta t) = \min\{x_{n-1}(t + \Delta t - \tau_n) - l_{n-1} - g_n^{jam}, x_n(t) + v_n(t)\Delta t + a_n^U \Delta t^2, x_n(t) + v_n^f \Delta t, x_n(t) + \Delta x_n^s(t + \Delta t)\} \tag{13}$$

$$\Delta x_n^s(t + \Delta t) = \Delta t\left(a_n^L \tau_n + \sqrt{(a_n^L \tau_n)^2 - 2a_n^L\left(x_{n-1}(t) - x_n(t) - l_{n-1} - g_n^{jam} - \frac{(x_{n-1}(t))^2}{2a_{n-1}^L}\right)}\right) \tag{14}$$

where τ_n is the reaction time of vehicle n; l_{n-1} is the length of vehicle $n-1$; g_n^{jam} is the jam spacing between vehicles n and $n-1$; $v_n(t)$ is the speed of the n^{th} vehicle at time t; a_n^U is the maximum acceleration of vehicle n; v_n^f is the free flow speed of vehicle n; $\Delta x_n^s(t + \Delta t)$ is the maximum safety distance to avoid collisions of vehicle n at time $t + \Delta t$; and a_n^L is the maximum deceleration of vehicle n.

The lower bound is determined by the deceleration capability and current position to prevent the vehicle moving backward. The lower bound travel distance is expressed as

$$x_n^L(t + \Delta t) = \max\{x_n(t), x_n(t) + v_n(t)\Delta t + a_n^L \Delta t^2\} \tag{15}$$

2.4. Signal control

The signal control is formulated as a DP problem which considers each phase as a stage in DP (Sen and Head, 1997). A forward recursion is used to calculate the performance measures and record the optimal value function. A backward recursion is used to retrieve the optimal solution.

The forward and backward recursions are described as follows.

Forward recursion

Step 1: Set $j = 1$ and $v_j(0) = 0$;
Step 2: for $s_j = 1, \ldots, T$

$$v_j(s_j) = Min_{x_j}\{f_j(s_j, x_j) + v_{j-1}(s_{j-1}) | x_j \in X_j(s_j)\} \tag{16}$$

Record $x_j^*(s_j)$ as the optimal solution in Step 2.

Step 3: if $(j < P + 1)$, $j = j + 1$, go to step 2.
else if $(v_{j-k}(T) = v_j(T))$ for all $k \le P - 1$, STOP.
Else $j = j + 1$, and go to step 2.

Where j is the stage (phase) index in DP; T is the total time in the planning horizon; P is the number of phases in one cycle; s_j is the state variable denoting the total number of time steps planned up to stage j; x_j is the control variable denoting the number of time steps planned in stage j; $X_j(s_j)$ is the set of feasible control variables given the total time planned s_j; $v_j(s_j)$ is the cumulative value function up to stage j given the total time planned s_j; and $f_j(s_j, x_j)$ is the performance function at stage j, given state variable s_j and control variable x_j.

The set of feasible control variables $X_j(s_j)$ depends on the signal parameters such as minimum green time, maximum green time, yellow change intervals and all-red clearance time. Let X_j^{min} and X_j^{max} to be the minimum phase time and maximum phase time of stage j, respectively. The minimum/maximum phase time includes the green, yellow and all-red clearance time of a phase. Then the feasible control variable set can be expressed:

$$X_j(s_j) = \begin{cases} 0, & \text{if } T - s_{j-1} \leqslant X_j^{min} \\ X_j^{min}, \ldots, X_j^{max}, & \text{if } T - s_{j-1} > X_j^{max} \\ X_j^{min}, \ldots, T - s_{j-1}, & \text{if } X_j^{min} \leqslant T - s_{j-1} \leqslant X_j^{max} \end{cases} \tag{17}$$

And $s_0 = 0$.

The performance function $f_j(s_j, x_j)$ is calculated based on total vehicle travel time delay. It is defined as the time difference between actual vehicle travel time and free flow travel time. The actual vehicle travel time is calculated by a vehicle's departure time at the stop bar minus the time when this vehicle enters the DSRC range. With vehicle trajectory control, no queue will be generated at the intersection unless under oversaturation. Vehicles may reduce their speeds in the upstream of the intersection, and the resultant delay is included in travel time delay calculation. Since the platoon leading vehicle's departure time is determined by the trajectory control algorithm, all following vehicles' departure time can be estimated by the saturation flow rate if a vehicle can catch up with its leading vehicle. Otherwise, the vehicle will arrive at the intersection with free flow speed (no delay). The algorithm plans as many stages (phases) as necessary to get the optimal solution until the stop criteria in step 3 is met. The proof of the stop criteria can be found in (Sen and Head, 1997).

Backward recursion

The backward recursion retrieves the optimal decision of each stage $x_j^*(s_j)$ working backwards.

Step1: $s_{J-1}^* = T$

Step2: for $\{j = J - 1, J - 2, \ldots, 1\}$

$$s_{j-1}^* = s_j^* - x_j^*(s_j) \tag{18}$$

where J is the total number of stages planned.

2.5. Benchmark model for objective function justification

To justify the simplified objective function in Eq. (5), the multi-scale motor vehicle & equipment emission system (MOVES) model (EPA, 2002) of U.S. Environmental Protection Agency (EPA) is applied as the benchmark model for comparison. This model estimates vehicle specific power (VSP) with the input from vehicle speed and acceleration values. Then VSP modes are identified through a look-up table. Furthermore, according to different types of vehicles, engine sizes, and mileages, vehicle emissions are located in the emission table (refer to the EPA report (EPA, 2002) for more details).

With the MOVES emission model as the objective function, the analytical solution is not available. Therefore, an approximation model (He et al., 2015) which transforms the optimal control problem to a nonlinear programming problem with much fewer decision variables is constructed for platoon leading vehicle trajectory control. The approximation model also divides a vehicle trajectory into three segments with constant acceleration or deceleration rates in each segment. The middle segment is for vehicle cruising where the vehicle speed is kept as a constant. Therefore, the decision variables in this model are reduced to four: two acceleration/deceleration rates a_1, a_2, and two switch time points t_1, t_2. The model is formulated as follows:

$$\min_{a_1,a_2,t_1,t_2} J = \int_0^{t_1} F(v(a_1,t),a_1)dt + \int_{t_1}^{t_2} F(v^c,0)dt + \int_{t_2}^{t_f} F(v(a_2,t),a_2)dt \tag{19}$$

s.t.

$$v^c = v_0 + a_1 t_1 = v_{tf} - a_2(t_f - t_2) \geqslant 0 \tag{20}$$

$$v_0 t_1 + \frac{1}{2}a_1 t_1^2 + v^c(t_2 - t_1) + v^c(t_f - t_2) + \frac{1}{2}a_2(t_f - t_2)^2 = L \tag{21}$$

$$0 \leqslant t_1 \leqslant t_2 \tag{22}$$

$$t_1 \leqslant t_2 \leqslant t_f \tag{23}$$

$$-a^L \leqslant a_1 \leqslant a^U \tag{24}$$

$$-a^L \leqslant a_2 \leqslant a^U \tag{25}$$

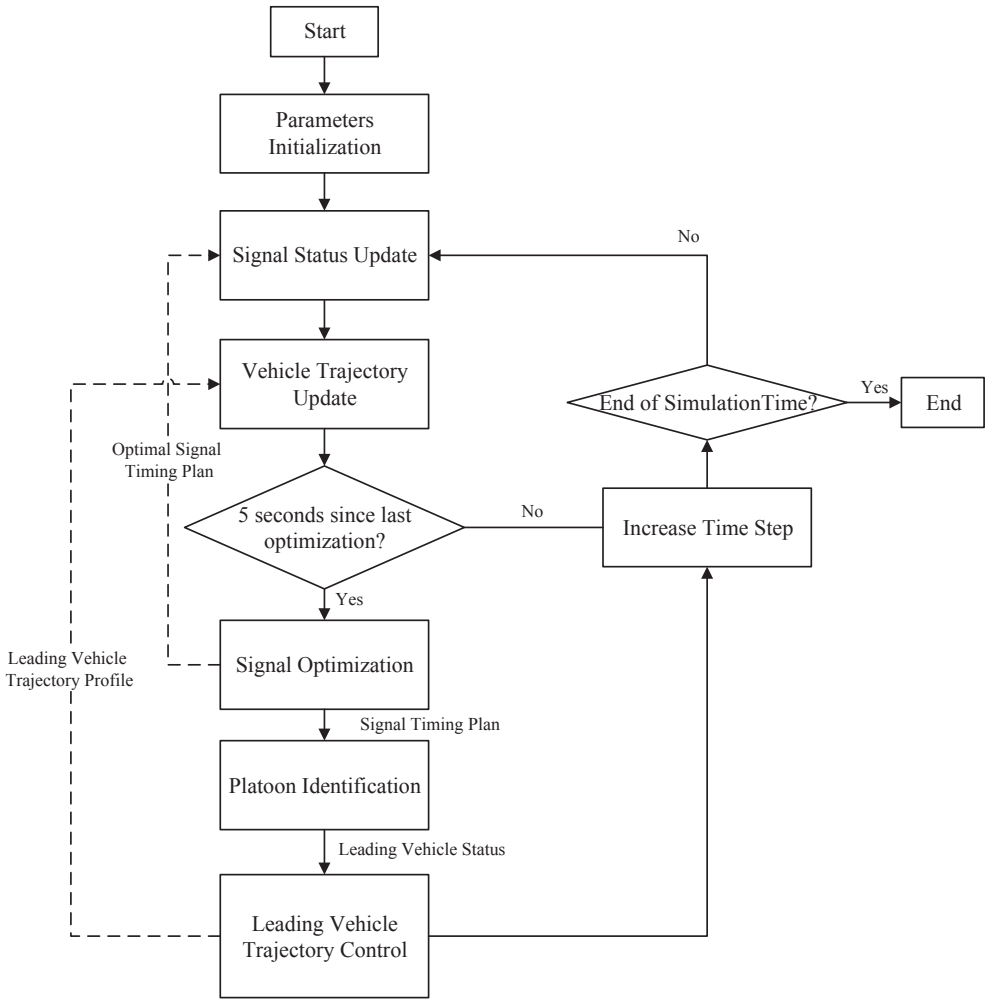

Fig. 5. Rolling horizon scheme.

In this formulation, $F(v, a)$ is the MOVES emission model and v^c is the cruising speed. Eq. (20) ensures that the vehicle speeds are continuous between trajectory segments. Eq. (21) ensures that the vehicle reaches the intersection at the end of the third trajectory segment. Eqs. (22)–(25) are the lower and upper boundaries of the decision variables.

This model doesn't require the maximum acceleration and deceleration rates during trajecotry planning. The cruising trajectory segment may not exist if $t_1 = t_2$. Although the formulation is simple and the number of decision variables is small, this problem is nonlinear which increases computational burden, and yet the quality of the solutions cannot be guaranteed, which is demonstrated in the numerical examples.

3. Rolling horizon scheme

The proposed joint control algorithm is implemented in MATLAB. The flow chart of the optimization process is shown in Fig. 5. Time is discretized into 1 s steps. Signal status and vehicle trajectories are updated every time step. A rolling horizon scheme is adopted in which the optimization process is repeated every 2 s to include recent vehicle arrivals. The planning horizon for signal optimization is two cycles, in which two cycles of signal timing are generated by DP. The generated signal timing will be executed in the next rolling horizon (2 s). It also serves as the input to the platoon identification algorithm. Then the optimal trajectories of the platoon leading vehicles are solved analytically using the optimal control model. Similarly, the platoon leading vehicles will follow the optimal trajectory during the next rolling horizon. Following vehicles update their trajectories according to the car-following model. Vehicle trajectories are used to estimate the performance function in signal optimization.

4. Numerical examples

4.1. Simulation setup

We start with a hypothetical intersection of two single-lane approaches. Two signal phases are applied, and no turning movements and lane changing behaviors are considered. The DSRC range is 300 m from the center of the intersection which provides reliable communication (Emmelmann et al., 2010). Although this paper assumes DSRC is used for V2I communication, other wireless communication technologies (e.g., cellular) can also be applied as long as the communication range and latency meet the requirement. All vehicles in the communication range are controllable, although only a few vehicles are controlled.

The default parameters for the car-following model are set as follows: $\tau_n = 2$ s, $l_{n-1} + g_n^{jam} = 6$ m (consider uniform vehicle length), $a_n^U = 2\,\text{m/s}^2$, $a_n^L = -2\,\text{m/s}^2$, $v_n^f = 14$ m/s ($\sim$50 km/h).

In signal optimization, the two phases of a cycle are identical. The corresponding default parameters are set as follows: the minimum green time $g_{min} = 10$, the maximum green time $g_{max} = 26$, and the transition interval $g_{tran} = 4$ which includes yellow interval and all-red clearance time. Therefore, $X_j^{min} = g_{min} + g_{tran}$ and $X_j^{max} = g_{max} + g_{tran}$. The maximum acceleration and deceleration rates for vehicle trajectory control are set to be the same as those in the car-following model, and $v_{tf} = 10$ m/s.

From the analysis in Appendix A, it can be seen that the optimal control formulation for leading vehicle trajectory control may not always have solutions. Based on the parameters above, if the green time generated by DP is smaller or equal to 5 s, the signal optimization will not be executed until the beginning of the next phase to prevent modifying the leading vehicle trajectory when it is too close to the intersection.

4.2. Simulation results and discussion

Vehicle arrival conforms to the Poisson distribution. Three different traffic demand levels are tested. The demands in the two approaches are set to be the same. The three levels are 500 veh/h/lane, 650 veh/h/lane and 800 veh/h/lane (i.e., medium, high and near-saturated traffic conditions). The corresponding v/c ratios are 0.64, 0.83, and 0.97. v/c ratio is calculated based on an 1800 veh/h/lane saturation flow rate and the effective green time is equal to the actual green time. Four different scenarios are simulated: Fixed, Adaptive, OC and NLP. In the “Fixed” scenario, vehicle trajectories are not controlled, and the signal timing is fixed. Each phase has 26 s of green time, 4 s of transition time and 30 s of red time. In the “Adaptive” scenario, vehicle trajectories are not controlled, but the signal timing is optimized using DP (Section 2.4). In the “OC” scenario, vehicle trajectories are controlled using the optimal control model with simplified objective function (Section 2.3.1) and the signal timing is optimized using DP. In the “NLP” scenario, vehicle trajectories are controlled using the Non-linear programming (NLP) approximation model with MOVES model as the objective function (Section 2.5) and the signal timing is optimized using DP. The total simulation time for each scenario is 1000 s. Fig. 6 shows the comparison of vehicle trajectories under the four scenarios with medium demand level. The DSRC communication range is shown as a horizontal line at the location of 200 m.

By comparing the scenarios “Fixed” and “Adaptive”, it can be seen that in some cycles of the “Fixed” scenario, a portion of green time is wasted. The “Adaptive” scenario generates timing plans adaptively based on vehicle arrivals so that green time will be utilized more efficiently. More specifically, under “Fixed” scenario, part of the green times are wasted during the fifth cycle and the seventh cycle, which does not occur with the “Adaptive” scenario. Without controlling vehicle trajectories, vehicles stop at stop-bars for red signals in both the “Fixed” and “Adaptive” scenarios. With vehicle trajectories controlled, leading vehicles of each platoon in the “OC” and “NLP” scenarios slowdown in the middle of the road segment to avoid stops at stop-bars. They are controlled to arrive at the intersection at the beginning of the green most of the times to improve green time utilization. Following vehicles obey the car-following model to catch up with preceding vehicles so that compact platoons are generated. The figure also shows that the scenarios “OC” and “NLP” generate similar vehicle trajectories. In both scenarios, at the end of the third cycle (around 150 s), there is a sudden deceleration of the leading vehicle trajectory. That’s caused by the change of signal timing due to adaptive signal control. In this case, the green time generated by the adaptive control algorithm is 1 s shorter than the previous rolling horizon. As a result, the last vehicle of the previous platoon cannot pass the intersection and it becomes the leading vehicle of a new platoon. It is then controlled to arrive at the intersection in the next cycle. On the other hand, the leading vehicle of the sixth cycle (around 270 s) cannot arrive at the intersection at the beginning of the green so that it is not controlled and it travels at the free-flow speed to the intersection.

Table 2 shows the comparison of total vehicle delay, CO_2 emissions and execution time of the four scenarios under different traffic demand levels. Results of all scenarios are the mean and standard deviation (value in parentheses) of 5 different random seeds. CO_2 emissions are calculated by the MOVES emission model based on vehicle trajectories generated in each scenario. Note that the “NLP” scenario incorporates MOVES model into the objective function while other three scenarios just use MOVES model for evaluation. Vehicle category 11 in MOVES model (odometer < 50,000 miles and engine size < 3.5 l) is used. The execution time to run the 1000 s simulation is recorded.

Several observations can be made from the results:

1. Without vehicle trajectory control, adaptive control outperforms fixed-time control regarding both vehicle delay and CO_2 emissions. The benefit decreases as traffic demand increases. That is because, under higher demand levels, adaptive control tends to assign maximum green time to each phase to serve more demand which essentially turns to be fixed-time control. With vehicle trajectory control, under near-saturated demand level, “OC” and “NLP” can still reduce about 10% vehicle delay compared to “Fixed” and “Adaptive”, because trajectory control eliminates start-up lost time and increases the capacity of the intersection. To

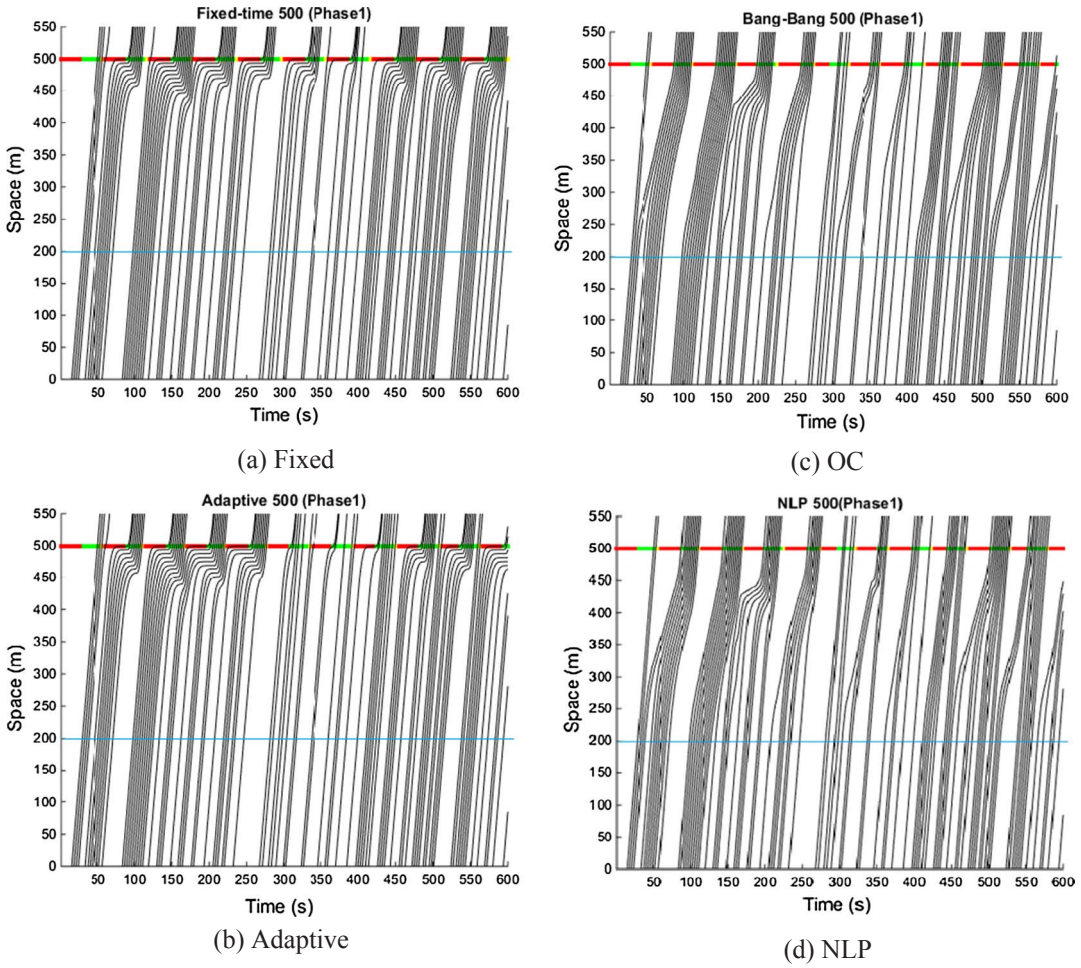

Fig. 6. Vehicle trajectory comparison under four scenarios.

Table 2
Comparison of vehicle delay, CO_2 emission and execution time.

Scenario	Delay (s)	%	CO_2 emission (kg)	%	Execution time (s)
Demand level: 500 veh/h/lane (v/c = 0.64)[a]					
Fixed	4400.6 (999.9)	N/A	51.4 (7.2)	N/A	0.8 (0.03)
Adaptive	3746.4 (749.3)	−14.9	47.5 (4.9)	−7.5	6.1 (0.14)
OC	3752.2 (854.5)	−14.7	47.2 (4.6)	−8.2	1.4 (0.06)
NLP	3851.4 (806.6)	−12.5	47.9 (4.1)	−6.7	657.8 (26.18)
Demand level: 650 veh/h/lane (v/c = 0.83)					
Fixed	15761.0 (2671.1)	N/A	113.5 (33.3)	N/A	1.1 (0.08)
Adaptive	14940.6 (2428.3)	−5.2	110.1 (32.4)	−2.9	6.3 (0.13)
OC	11981.6 (2095.7)	−24.0	97.9 (26.3)	−13.8	1.6 (0.11)
NLP	12056.0 (2143.6)	−23.5	99.1 (27.3)	−12.6	886.6 (82.89)
Demand level: 800 veh/h/lane (v/c = 0.97)					
Fixed	31729.2 (2255.9)	N/A	159.6 (14.36)	N/A	1.7 (0.07)
Adaptive	31549.0 (2541.1)	−0.6	157.0 (13.77)	−1.6	6.6 (0.08)
OC	28381.4 (2116.5)	−10.6	150.1 (9.1)	−6.0	2.3 (0.11)
NLP	27635.8 (1996.4)	−12.9	150.4 (9.0)	−5.8	1529.9 (111.23)

[a] v/c ratio is calculated assuming an 1800 veh/h/lane saturation flow rate and effective green time is equal to actual green time.

better illustrate the benefit of capacity increase, we design a special case with uniform vehicle arrival (800 veh/h/lane) and fixed-time signals as shown in Fig. 7. It can be seen from Fig. 7(a) that, without trajectory control, the intersection is oversaturated and the queue is propagating over cycles. Fig. 7(b) shows the vehicle trajectories under the same demand level and the same signal

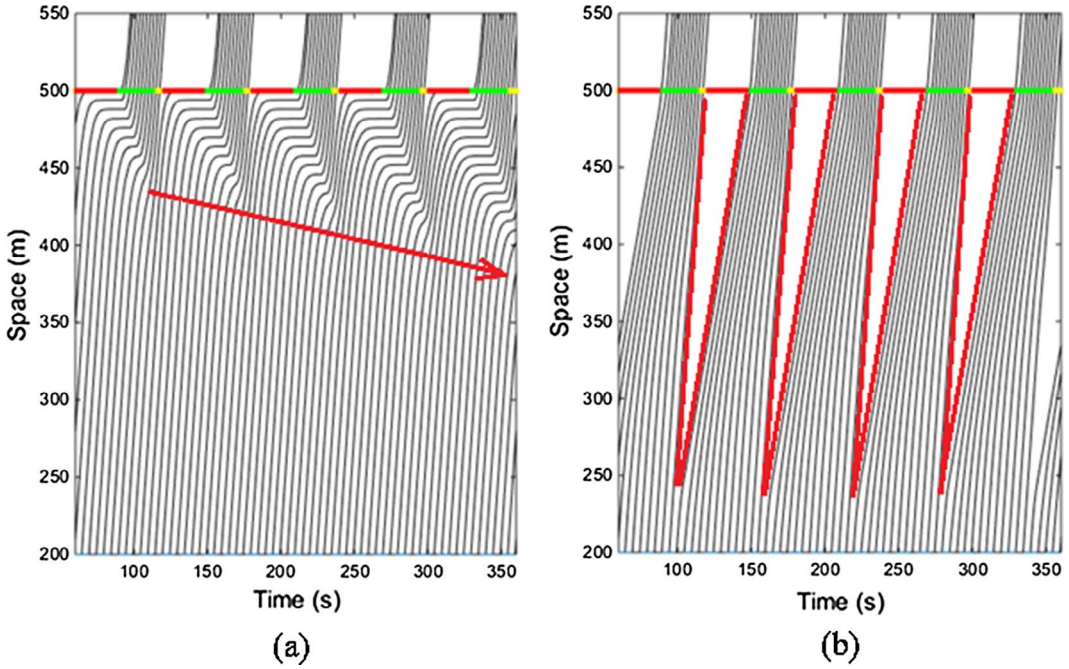

Fig. 7. Capacity increase with trajectory control.

plan. The gaps between each trajectory block remain the same over cycles, which suggests no oversaturation in this case. It is well known that vehicle delay increases dramatically under oversaturated traffic conditions, which can be avoided because of the increased capacity.

2. Both vehicle delay and emissions are reduced in the "OC" and "NLP" scenarios compared to the "Fixed" and "Adaptive" scenarios by as much as 24.0% and 13.8%, respectively. More benefits are shown under high demand levels. Compared to medium and near-saturated demand levels, both signal optimization and vehicle trajectory control have more flexibility in terms of green time allocation and intersection capacity utilization.
3. The vehicle delays in the "OC" and "NLP" scenarios are similar. But the "OC" scenario generates lower emissions than the "NLP" scenario in all cases. In both vehicle trajectory optimization problems, vehicle delay is formulated as a constraint, because the arrival time at the intersection is fixed through trajectory control. As long as a feasible solution can be found, both problems generate similar vehicle delays. However, emissions are formulated as the objective function, whose value depends on the quality of the solution. The approximation model is an NLP problem, and no global optimality is guaranteed. In spite of the simplified objective function in the optimal control formulation, the analytical solutions still outperform those generated using the emission model as the objective function.
4. The execution time differs among the four scenarios. The "Fixed", "Adaptive", and "OC" scenarios have similar execution times while the "NLP" scenario requires significantly longer time. In the "NLP" scenario, a long execution time is observed due to the difficulty in dealing with nonlinearity. On the contrary, the analytical solution from the optimal control formulation reduces computational time notably.

The results have validated the use of the simplified objective function instead of the exact but complex emission model in terms of both computational time and solution performance.

4.3. Sensitivity analysis

In the vehicle trajectory control, the final speed (v_{t_f}) and the maximum acceleration/deceleration rate (a^U/a^L) are the most important parameters. To further analyze the impacts of these parameters, two sensitivity analyses are performed.

In the first sensitivity analysis, v_{t_f} varies from 5 m/s to 14 m/s with an increment of 1 m/s. The maximum final speed is 14 m/s, the same as the free flow speed. The three demand levels are tested as shown in Fig. 8. When the demand level is 500 veh/h/ln (Fig. 8(a)), final speeds have no significant impacts on vehicle delay. This is because the time gaps between subsequent vehicles are relatively large and the lower flow rate caused by lower final speed of the leading vehicle can be easily absorbed by the gaps. As a result, following vehicles are not impacted. When demand increases and the final speed is low, as shown in Fig. 8(b) and (c), average vehicle delay increases significantly. Another reason is that a lower final speed of the leading vehicle actually lowers the intersection capacity, which has more significant influence under higher demand levels. However, the average vehicle delay remains stable at different demand levels when the final speed is greater or equal to 7 m/s, which shows a good stability of the proposed model.

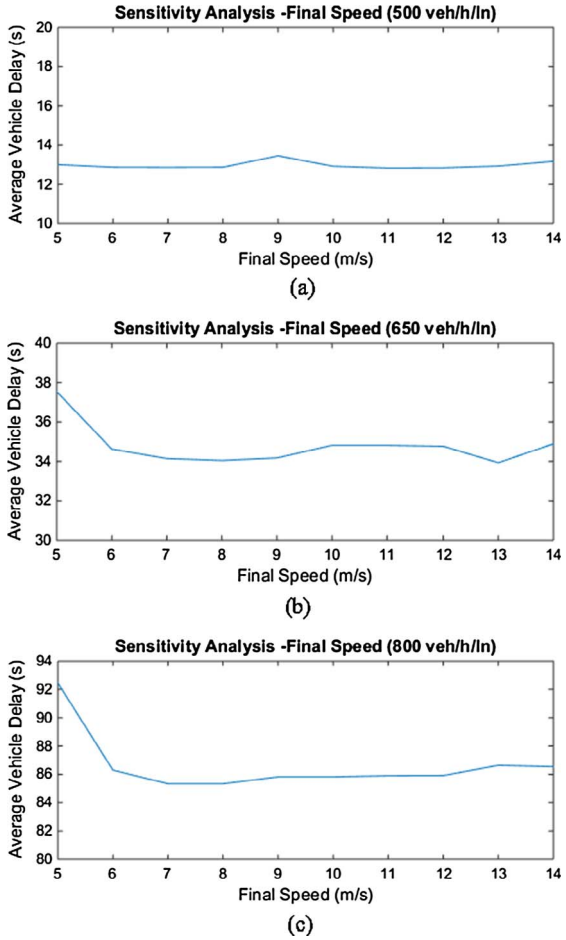

Fig. 8. Sensitivity analysis on final speed.

The maximum acceleration and deceleration rates influence both the controllability and the comfort of vehicle occupants. In the second sensitivity analysis, the absolute value of acceleration and deceleration rates vary from 0.6 m/s^2 to 2.4 m/s^2 with an increment of 0.2 m/s^2. Fig. 9 shows average vehicle delay and CO_2 emissions with different acceleration and deceleration rates under 650 veh/h/ln demand level. Results show that both vehicle delay and emissions increase with the decrease of the absolute value of maximum acceleration. When the absolute value decreases, the controllability of the vehicle trajectory also decreases. It is more difficult to control the platoon leading vehicle to the same final speed at the beginning of green. The opposing phase may need to extend the green time by a few seconds longer to leave enough time for the leading vehicle trajectory control of the current phase, so

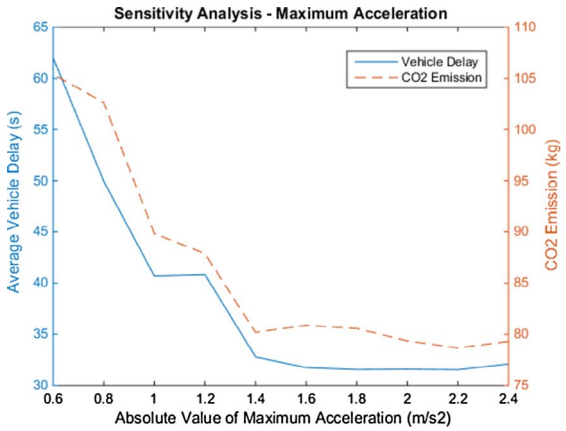

Fig. 9. Sensitivity analysis on acceleration rate.

Table 3
Comparison of vehicle delay, CO_2 emission of a standard eight phase intersection.

Scenario	Delay (s)	%	CO_2 emission (kg)	%
Demand level: 150/400/100/300				
Adaptive	16313.6 (1223.3)	N/A	136.4 (8.4)	N/A
OC	15508.2 (1138.6)	−4.9	129.7 (8.0)	−4.9
Demand level: 175/450/125/350				
Adaptive	25637.4 (3627.9)	N/A	185.1 (18.7)	N/A
OC	22979.2 (3637.4)	−10.4	173.0 (18.9)	−6.5
Demand level: 200/500/150/400				
Adaptive	37138.8 (4622.1)	N/A	237.8 (25.8)	N/A
OC	32642.6 (4246.9)	−12.1	216.6 (21.6)	−8.9
Demand level: 225/550/175/450				
Adaptive	55467.0 (4617.2)	N/A	327.1 (23.5)	N/A
OC	48153.8 (4900.3)	−13.2	292.4 (22.3)	−10.6

that signal timing may not be optimal. However, with a lower maximum acceleration rate, vehicle occupants feel more comfortable. A trade-off must be made between comfortability and efficiency.

4.4. Extension to standard intersection

We further extend the proposed spatiotemporal control framework to a standard intersection with eight phases following the dual-ring barrier structure. We assume that vehicles of different movements are generated on their target lanes so that lane changings are not needed. From the analysis of the simple two-phase intersection, it can be seen that fixed-time control has significantly worse performance than adaptive control. NLP generates very similar vehicle trajectories with the optimal control but needs much longer execution time. As a result, we only compare adaptive control (Adaptive) and optimal control (OC) for the standard intersection. The baseline traffic demand levels are set to 150 veh/h/lane for phase 1 and 5, 400 veh/h/lane for phase 2 and 6, 100 veh/h/lane for phase 3 and 7, and 300 veh/h/lane for phase 4 and 8. Note that the traffic demands are not balanced for the two arterials. To simulate different traffic demand levels, the volume of each phase is incremented every 25 veh/h/lane for left turn phases and 50 veh/h/lane for through phases. Totally four demand levels are generated. Other simulation parameters are set to be the same as in Section 4.1. Table 3 shows the comparison of total vehicle delay, and CO_2 emissions of the two scenarios under different traffic demand levels. Results of all scenarios are the mean and standard deviation (value in parentheses) of five different random seeds. From Table 3, we can see a similar pattern that the joint control method performs better under higher demand levels than lower demand levels. Both of the delay and the CO_2 emission reduction increase with the traffic demand. Note that when DP is utilized for signal optimization, the optimization execution time of the eight-phase intersection does not increase significantly compared to the two-phase intersection. However, enumeration method used in the previous study (Li et al., 2014) becomes very inefficient since the complexity increases exponentially with the number of phases.

5. Conclusions and further research

In this paper, we propose a joint control framework for controlling vehicle trajectories and traffic signals simultaneously to improve the efficiency of intersection operation as well as reduce vehicle emissions in a CAV environment. The control is extended from one dimension (either spatial or temporal) to two dimensions (spatiotemporal). The joint control framework is formulated as a two-stage optimization model. A simplified objective function is proposed in the vehicle trajectory control model to obtain analytical solutions. Therefore, the two-stage problem can be solved efficiently. Only platoon leading vehicles are controlled. Simulation results show that the proposed joint control framework is able to reduce both vehicle delay and emissions under a variety of demand levels. The simplified objective function is validated, which generates comparable results to the MOVES emission model but with significantly reduced computational time.

This paper provides a theoretical foundation for controlling traffic signals and vehicle trajectories cooperatively. Trajectories generated from the proposed model can be considered at a strategic level and served as the input to lower level vehicle models which consider mass and powertrain. One of the major work for further research is to focus on the mixed traffic condition where not all vehicles are controllable. It is also the main reason why a leading vehicle control strategy is proposed, so that it can be extended to the mixed traffic condition more easily.

Acknowledgements

This research was partially funded by the U.S. Department of Energy (EERE Award No. DE-EE0007212). The views presented in this paper are those of the authors alone.

Appendix A

The PMP is applied to derive the analytical solution of the optimal control problem with Eq. (5) as the objective function and Eqs. (6)–(9) as the constraints.

The Hamiltonian function is introduced:

$$H(\boldsymbol{X}(t),\boldsymbol{\lambda}(t),u(t)) = F(v(t),u(t)) + \boldsymbol{\lambda}(t)\cdot f(\boldsymbol{X}(t),u(t)) = |u(t)| + \lambda_x(t)v(t) + \lambda_v(t)u(t) \tag{26}$$

where $\boldsymbol{\lambda}(t) = [\lambda_x(t),\lambda_v(t)]$. is the Lagrange multiplier vector and its elements are the costates of the system; $\boldsymbol{X}(t) = [x(t), v(t)]^T$ is the state vector.

Based on the problem, the PMP states that the optimal state trajectory $\boldsymbol{X}^*(t)$ and the optimal control $u^*(t)$ should fulfill the following conditions (27)–(29):

$$\begin{cases} \dot{\lambda}_x(t) = -\frac{\partial H}{\partial x} = 0 \\ \dot{\lambda}_v(t) = -\frac{\partial H}{\partial v} = -\lambda_x(t) \end{cases} \tag{27}$$

$$|u^*(t)| + \lambda_v(t)u^*(t) \leqslant |u(t)| + \lambda_v(t)u(t), u(t) \in [-a_L, a_U] \tag{28}$$

$$|u^*(t)| + \lambda_x(t)v^*(t) + \lambda_v(t)u^*(t) = |u^*(t)| + \lambda_x(t_f)v^*(t_f) + \lambda_v(t_f)u^*t_f) = Const \tag{29}$$

The optimal control $u^*(t)$ which depends on costate $\lambda_v(t)$ can be derived from Eq. (28). If $\lambda_v(t) < -1$, then only $u^*(t) = a^U$ can satisfy Eq. (28). If $\lambda_v(t) > 1$, then only $u^*(t) = -a^L$ can satisfy Eq. (28). If $|\lambda_v(t)| < 1$, then only $u^*(t) = 0$ can satisfy Eq. (28). If $\lambda_v(t) = 1$, then any non-positive value of $u^*(t)$ can satisfy Eq. (28). Similarly, if $\lambda_v(t) = -1$, then any non-negative value of $u^*(t)$ can satisfy Eq. (28). In summary, the optimal control $u^*(t)$ can be expressed in Eq. (30) and Fig. 10.

$$u^*(t) = \begin{cases} 0, & |\lambda_v(t)| < 1 \\ -a^L, & \lambda_v(t) > 1 \\ a^U, & \lambda_v(t) < -1 \\ [-a^L, 0], & \lambda_v(t) = 1 \\ [0, a^U], & \lambda_v(t) = -1 \end{cases} \tag{30}$$

To further analysis the optimal control trajectory, the costates expressed in the partial differential equations can be solved as

$$\lambda_x(t) = \lambda_x(0) = C \tag{31}$$

$$\lambda_v(t) = \lambda_v(0) - \lambda_x(0)t \tag{32}$$

Based on the values of the costates, two different control situations: ordinary control and singular control can be identified.

A.1. Situation I: Singular control

If $\lambda_x(t) = \lambda_x(0) = 0$, then $\lambda_v(t) = \lambda_v(0)$ is a constant. From Eq. (29), we can get

$$|u^*(t)| + \lambda_v(t)u^*(t) = Const \tag{33}$$

If $\lambda_v(t) = 1$ or $\lambda_v(t) = -1$, then $u^*(t)$ can be any non-positive or non-negative values within the boundaries and Eq. (33) is constantly

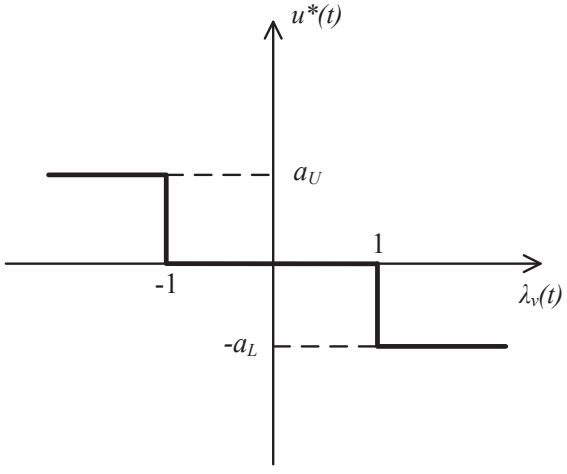

Fig. 10. Optimal control solution.

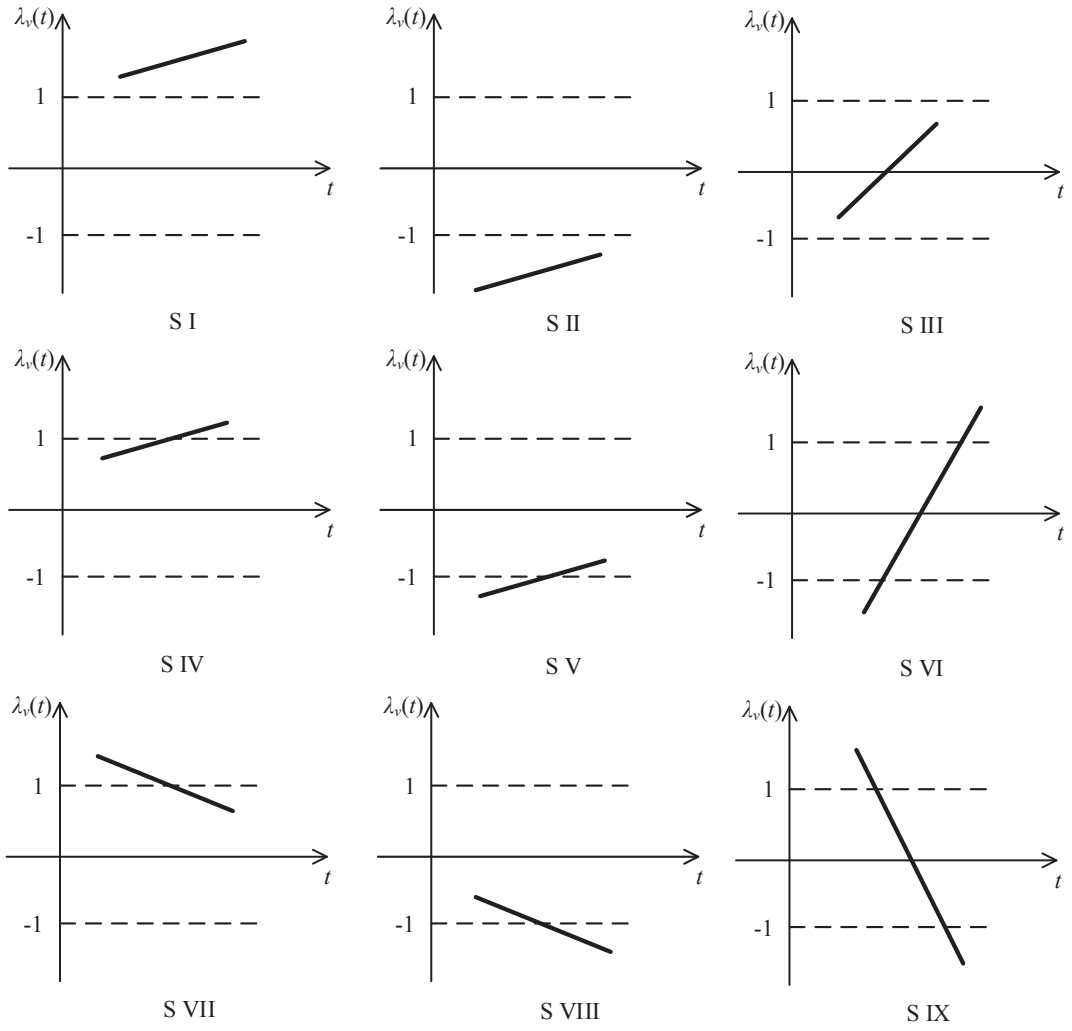

Fig. 11. Ordinary control – nine scenarios.

to be zero in both cases.

To present the optimal control in the cases when $\lambda_v(t) = 1$ or $\lambda_v(t) = -1$, we define a set of non-negative continuous functions:

$$W^+ = \{w(t)|0 \leqslant w(t) \leqslant a \ ,\forall\ t \in [0,t_f]\} \tag{34}$$

The optimal control $u^*(t)$ can be presented as

$$u^*(t) = -sgn\{\lambda_v(0)\}w(t) \tag{35}$$

where $sgn\{\}$ is the sign function, $a = a^U$ if $\lambda_v(t) = -1$ and $a = a^L$ if $\lambda_v(t) = 1$.

A.2. Situation II: Ordinary control

If $\lambda_x(t) = \lambda_x(0) \neq 0$, then $\lambda_v(t) = \lambda_v(0) - \lambda_x(0)t$ which is a linear function of time t. Nine control scenarios (S I to S IX) can be identified based on the initial and final values of $\lambda_v(t)$ as shown in Fig. 11. The nine scenarios are expressed below:

S I: $\{-a^L\}$	S II: $\{a^U\}$	S III: $\{0\}$
S IV: $\{0, -a^L\}$	S V: $\{a^U, 0\}$	S VI: $\{a^U, 0, -a^L\}$
S VII: $\{-a^L, 0\}$	S VIII: $\{0, a^U\}$	S IX: $\{-a^L, 0, a^U\}$

Three ranges of $\lambda_v(t)$ are identified based on the critical values in Eq. (30): $\lambda_v(t) > 1$, $\lambda_v(t) < -1$, $|\lambda_v(t)| < 1$. For example, in control scenario S IV, the value of $\lambda_v(t)$ starts from the range where $|\lambda_v(t)| < 1$ and ends with the range where $\lambda_v(t) > 1$. As a result, two segments can be identified: constant speed and deceleration. It can be seen from the figure that at most three-segment control

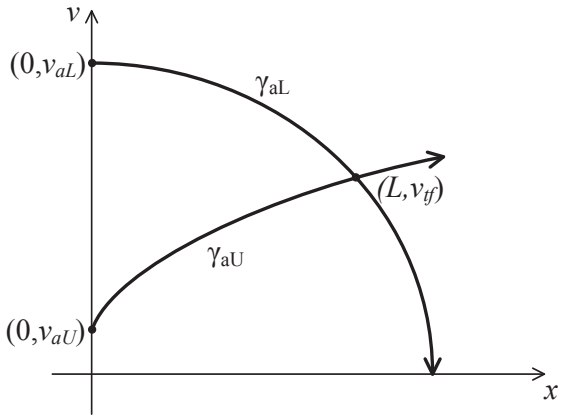

Fig. 12. Phase plane diagram of the system.

scenario can be identified (S VI and S IX). The number of segments can also be two (S IV, S V, S VII, S VIII) or one (S I, S II, S III).

If $\lambda_x(t) = \lambda_x(0) = 0$ and $\lambda_v(t) = const \neq \pm 1$, then the value of $u^*(t)$ is fixed which keeps Eq. (33) a constant. Depending on the value of $\lambda_v(t)$, the optimal control belongs to scenarios S I, S II or S III.

To further analyze different control cases, the phase plane diagram is drawn under different initial states and transition times. The phase plane diagram of the system is shown in Fig. 12.

γ_{aL} and γ_{aU} are state trajectories passing the final state (L, v_{tf}) with scenarios S I: $\{-a^L\}$ and S II: $\{a^U\}$ respectively, which serve as the boundary trajectories (maximum acceleration and maximum deceleration all the time). v_{a^L} and v_{a^U} are the initial vehicle speeds if the control trajectories follows the boundary trajectories and they can be calculated as

$$v_{a^L} = \sqrt{2La^L + v_{tf}^2} \tag{36}$$

$$v_{a^U} = \sqrt{v_{tf}^2 - 2La^U} \text{ (assume } v_{tf}^2 - 2La^U \geqslant 0) \tag{37}$$

Based on different initial state $(0, v_0)$, and transition time t_f, different cases and their corresponding optimal control trajectories are investigated.

Case 1: $v_0 > v_{a^L}$ or $v_0 < v_{a^U}$

No feasible solution can be found in Case 1. It is obvious that if the initial speed of the vehicle is too fast or too slow, even with maximum deceleration or acceleration, the vehicle is not able to reach the final state. In fact, any initial states that are out of the area surrounded by points $(0, v_{a^L})$, $(0, v_{a^U})$ and (L, v_{tf}), can't be transited to the final state.

Case 2: $v_0 = v_{a^L}$

Case 2.1 $t_f = t_{a^L}^{cri}$

If $v_0 = v_{a^L}$, the feasible control trajectory may exist if $t_f = \frac{v_{a^L} - v_{tf}}{a^L}$, noted as $t_{a^L}^{cri}$. $t_{a^L}^{cri}$ is the minimum time required to reduce the initial speed v_0 to the final speed v_{tf}. In this case, control scenario S I: $\{-a^L\}$ is applicable. The state trajectory of this control scenario is shown in Fig. 13(a).

Case 2.2 $t_f \neq t_{a^L}^{cri}$

If $v_0 = v_{a^L}$ and $t_f \neq t_{a^L}^{cri}$, then no feasible solution can be found since the distance will exceed the final position ($t_f > t_{a^L}^{cri}$) or the speed can't be reduced to the final speed ($t_f < t_{a^L}^{cri}$).

Case 3: $v_{tf} < v_0 < v_{a^L}$

In this case, at least two control segments are required.

Case 3.1 $t_f = t_{a^L}^{L}$

$t_{a^L}^{L}$ is defined as the lower time boundary (minimum time) to reach the final state **without** acceleration. This case results in control scenario S IV: $\{0, -a^L\}$, which maintains a higher constant speed segment at first with a shorter transition time. The state

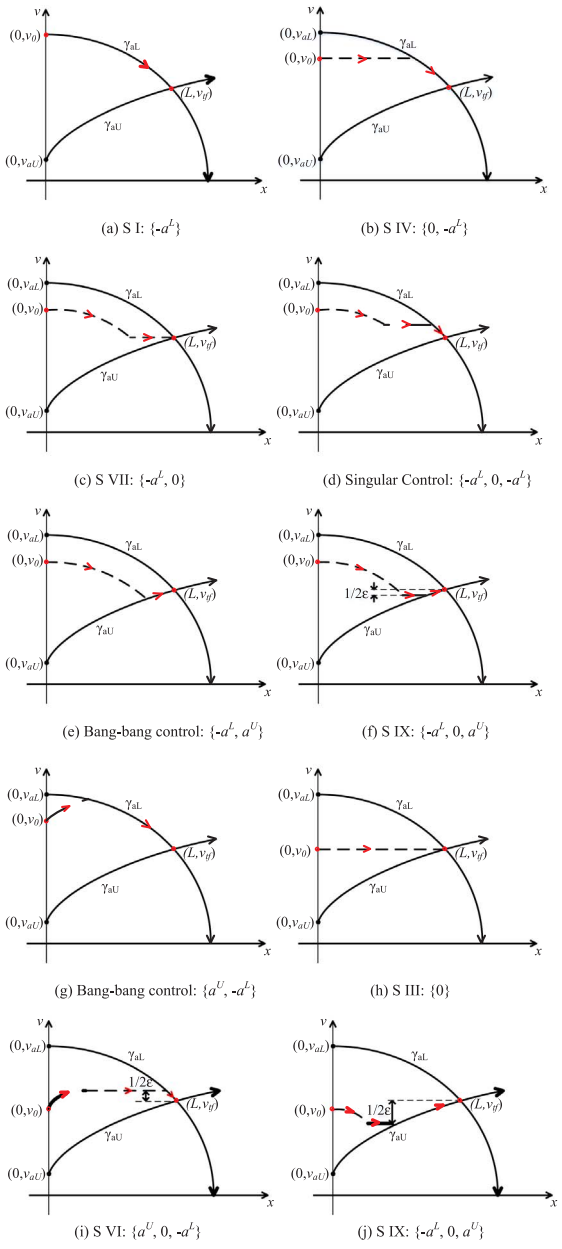

Fig. 13. Phase plane diagram under different control scenarios.

trajectory of this control scenario is shown in Fig. 13(b). $t_{a^L}^{L} = \frac{L}{v_0} + \frac{(v_0 - v_{tf})^2}{2v_0 a^L}$ can be solved based on the following equations:

$$t_s = \frac{v_0 - v_{tf}}{a^L} \tag{38}$$

$$t_c = t_f - t_s \tag{39}$$

$$d_s = v_0 t_s - \frac{1}{2} a^L t_s^2 \tag{40}$$

$$d_c = v_0 t_c \tag{41}$$

$$d_s + d_c = L \tag{42}$$

where t_s and t_c are the time spent in the deceleration segment and constant speed segment, respectively; d_s and d_c are the distances traveled in the deceleration segment and constant speed segment, respectively.

Case 3.2 $t_f = t_{a^L}^{U}$

$t_{a^L}^{U}$ is defined as the upper time boundary (maximum time) to reach the final state **without** decelerating below the final speed v_{tf}. This results in control scenario S VII: $\{-a^L, 0\}$, which has a lower constant speed segment with a longer transition time. The state trajectory of this control scenario is shown in Fig. 13(c). $t_{a^L}^{U} = \frac{L}{v_{tf}} - \frac{(v_0 - v_{tf})^2}{2v_{tf}a^L}$ can be calculated similarly as $t_{a^L}^{L}$.

Case 3.3 $t_{a^L}^{L} < t_f < t_{a^L}^{U}$

In this case, two-segment control can't transit vehicle trajectory from the initial state to the final state, three-segment control scenario such as $\{-a^L, 0, -a^L\}$ is required as shown in Fig. 13(d). The control scenario in this case doesn't belong to any of the nine scenarios in ordinary control. The deceleration rate switches between $-a^L$ and 0 which only belongs to the singular control situation. The speed of the constant speed segment should be between v_0 and v_{tf} in order to fulfill the transition time requirement. The number of control segments is flexible since the singular control can switch multiple times between $-a^L$ and 0. However, if three-segment control is implemented, then the switch time t_1 and t_2 can be solved uniquely with the constraint of $t_1 < t_2$ as shown in Fig. 3 and Eqs. (10) and (11). Similar calculation can also be applied to other three-segment scenarios (e.g. S IX: $\{-a^L, 0, a^U\}$). If more than three segments are implemented, then more equations need to be solved which increases the complexity, but doesn't improve the quality of the solution. As a result, in this study, we limit the number of trajectory segments to be at most three segments. In fact, control scenario $\{0, -a^L, 0\}$ is also a feasible singular control scenario and it is optimal.

Case 3.4: $t_{a^L}^{U} < t_f \leqslant t_{fea}^{U}$

t_{fea}^{U} is defined as the upper boundary of transition time when a feasible solution exists. The state trajectory when $t_f = t_{fea}^{U}$ is shown in Fig. 13(e). It is a two-segment control with a maximum deceleration segment followed by a maximum acceleration segment to maximize the transition time. This is a bang-bang control scenario $\{-a^L, a^U\}$ which neither belongs to ordinary control nor singular control. If the transition time $\underline{tf}$ is strictly smaller than t_{fea}^{U}, then the control scenario is a three-segment control S IX: $\{-a^L, 0, a^U\}$ as shown in Fig. 13(f). However, both of the control scenario S IX and bang-bang control are not optimal. Intuitively, the vehicle has to decelerate below the final speed and then accelerate which results in more speed fluctuation. The objective function calculated from this control scenario is greater than the optimal value J^* by ε, which is ε-optimal control: given an initial state $(0, v_0)$ and a final state (L, v_{tf}), if a feasible control trajectory exists and the value of its corresponding objective function is $\varepsilon + J^*$.

Case 3.5: $t_{fea}^{L} \leqslant t_f < t_{a^L}^{L}$

t_{fea}^{L} is defined as the lower boundary of transition time when a feasible solution exists. The trajectory when $t_f = t_{fea}^{L}$ is shown in Fig. 13(g). It is a two-segment control with a maximum acceleration segment followed by a maximum deceleration segment to minimize the transition time. Similar with the previous case, this solution is a bang-bang control scenario $\{a^U, -a^L\}$. When the transition time $\underline{tf}$ is strictly greater than t_{fea}^{L} then the control scenario is a three-segment control S VI: $\{a^U, 0, -a^L\}$. Again, both of them are not optimal control, but ε-optimal control.

Case 3.6: $t_{fea}^{L} > t_f$ or $t_{fea}^{U} < t_f$

No feasible solution can be found in this case.

Case 4: $v_0 = v_{tf}$
Case 4.1: $t_f = L/v_0$

In this case, the vehicle only needs to keep a constant speed, and no acceleration or deceleration is required. One-segment control scenario S III: $\{0\}$ is applicable as shown in Fig. 13(h).

Case 4.2: $t_{fea}^{L} \leqslant t_f \leqslant L/v_0$

In this case, the vehicle needs to accelerate and then decelerate to fulfill the transition time constraint. Therefore, the three-segment ε-optimal control S VI: $\{a^U, 0, -a^L\}$ or the two-segment bang-bang control $\{a^U, -a^L\}$ are applicable. The ε-optimal control is shown in Fig. 13(i).

Case 4.3: $L/v_0 \leqslant t_f \leqslant t_{fea}^{U}$

In this case, the vehicle needs to decelerate and then to accelerate to fulfill the transition time constraint. Therefore, the three-segment ε-optimal control S IX: $\{-a^L, 0, a^U\}$ or the two-segment bang-bang control $\{-a^L, a^U\}$ are applicable. The ε-optimal control is shown in Fig. 13(j).

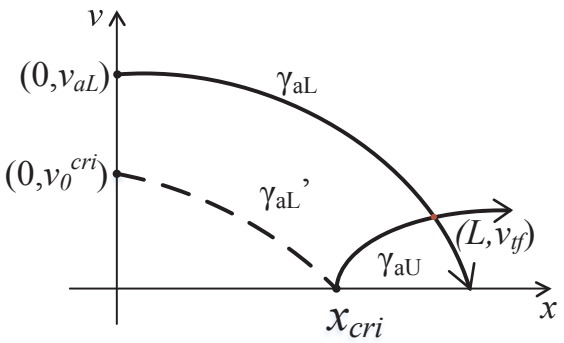

Fig. 14. Phase plane diagram when transition time has no upper boundary.

Case 4.4: $t_{fea}^{L} > t_f$ or $t_{fea}^{U} < t_f$

No feasible solution can be found in this case.

Case 5: $v_{a^U} \leqslant v_0 < v_{tf}$

The scenarios in Case 5 are similar to Case 3. To avoid redundancy, the analysis of Case 5 is skipped.

All previous cases assume that $v_{a^U} = \sqrt{v_{tf}^2 - 2La^U} \geqslant 0$. In fact, if the final location L is far away and/or the final speed v_{tf} is low, the trajectory γ_{aU} may intersect with x axis instead of v axis as shown in Fig. 14. The intersection point is noted as x_{cri} which can be calculated as

$$x_{cri} = L - v_f^2/2a^U \tag{43}$$

Let the trajectory with maximum deceleration rate $-a^L$ and passing x_{cri} be γ_{aL}'. γ_{aL}' intersects with v axis at $(0, v_0^{cri})$, where

$$v_0^{cri} = \sqrt{2La^L - v_f^2 a^L/a^U} < v_{a^L} \tag{44}$$

If $v_0 \leqslant v_0^{cri}$, then the transition time t_f doesn't have an upper boundary since the vehicle speed can drop to (near) zero and the cruise time (constant speed) can be very long. That means t_f can be greater than t_{fea}^U. The control strategies in this case is similar to previous analysis expect that the constraint $t_{fea}^U \geqslant t_f$ can be released.

It is noted that in some cases, the feasible control solution doesn't exist. Section 4 provides the illustration ofhow to prevent such conditions by limiting the control distance.

References

Benson, D.A., Huntington, G.T., Thorvaldsen, T.P., Rao, A.V., 2006. Direct trajectory optimization and costate estimation via an orthogonal collocation method. J. Guid. Control Dyn. 29, 1435–1440. http://dx.doi.org/10.2514/1.20478.

Datesh, J., Scherer, W.T., Smith, B.L., 2011. Using k-means clustering to improve traffic signal efficacy in an IntelliDriveSM environment. In: 2011 IEEE Forum on Integrated and Sustainable Transportation System (FISTS). Presented at the 2011 IEEE Forum on Integrated and Sustainable Transportation System (FISTS), pp. 122–127. http://doi.org/10.1109/FISTS.2011.5973659.

Emmelmann, M., Bochow, B., Kellum, C., 2010. Vehicular Networking: Automotive Applications and Beyond. John Wiley & Sons.

EPA, 2002. Methodology for Developing Modal Emission Rates for EPA's Multi-Scale Motor Vehicle and Equipment Emission System (No. EPA420-R-2–27).

Feng, Y., Head, K.L., Khoshmagham, S., Zamanipour, M., 2015. A real-time adaptive signal control in a connected vehicle environment. Transp. Res. Part C: Emerg. Technol. 55, 460–473. http://dx.doi.org/10.1016/j.trc.2015.01.007.

Garg, D., Patterson, M., Hager, W.W., Rao, A.V., Benson, D.A., Huntington, G.T., 2010. A unified framework for the numerical solution of optimal control problems using pseudospectral methods. Automatica 46, 1843–1851. http://dx.doi.org/10.1016/j.automatica.2010.06.048.

Gipps, P.G., 1981. A behavioural car-following model for computer simulation. Transp. Res. Part B: Methodol. 15, 105–111. http://dx.doi.org/10.1016/0191-2615(81)90037-0.

Goodall, N., Smith, B., Park, B., 2013. Traffic signal control with connected vehicles. Transp. Res. Rec. J. Transp. Res. Board 2381, 65–72. http://dx.doi.org/10.3141/2381-08.

Gradinescu, V., Gorgorin, C., Diaconescu, R., Cristea, V., Iftode, L., 2007. Adaptive traffic lights using car-to-car communication. In: Vehicular Technology Conference, 2007. VTC2007-Spring. IEEE 65th. Presented at the Vehicular Technology Conference, 2007. VTC2007-Spring. IEEE 65th, pp. 21–25. http://doi.org/10.1109/VETECS.2007.17.

He, Q., Head, K.L., Ding, J., 2012. PAMSCOD: Platoon-based arterial multi-modal signal control with online data. Transp. Res. Part C: Emerg. Technol. 20, 164–184. http://dx.doi.org/10.1016/j.trc.2011.05.007.

He, X., Liu, H.X., Liu, X., 2015. Optimal vehicle speed trajectory on a signalized arterial with consideration of queue. Transp. Res. Part C: Emerg. Technol. 61, 106–120. http://dx.doi.org/10.1016/j.trc.2015.11.001.

Lee, J., Park, B., 2012. Development and evaluation of a cooperative vehicle intersection control algorithm under the connected vehicles environment. IEEE Trans. Intell. Transp. Syst. 13, 81–90. http://dx.doi.org/10.1109/TITS.2011.2178836.

Lee, J., Park, B., Yun, I., 2013. Cumulative travel-time responsive real-time intersection control algorithm in the connected vehicle environment. J. Transp. Eng. 139, 1020–1029. http://dx.doi.org/10.1061/(ASCE)TE.1943-5436.0000587.

Li, Z., Elefteriadou, L., Ranka, S., 2014. Signal control optimization for automated vehicles at isolated signalized intersections. Transp. Res. Part C: Emerg. Technol. 49, 1–18. http://dx.doi.org/10.1016/j.trc.2014.10.001.

Ma, J., Li, X., Zhou, F., Hu, J., Park, B.B., 2016. Parsimonious shooting heuristic for trajectory design of connected automated traffic part II: computational issues and optimization. Transp. Res. Part B: Methodol.

Newell, G.F., 2002. A simplified car-following theory: a lower order model. Transp. Res. Part B: Methodol. 36, 195–205. http://dx.doi.org/10.1016/S0191-2615(00)00044-8.

Rao, A.V., Benson, D.A., Darby, C., Patterson, M.A., Francolin, C., Sanders, I., Huntington, G.T., 2010. Algorithm 902: GPOPS, A MATLAB software for solving multiple-phase optimal control problems using the Gauss pseudospectral method. ACM Trans. Math. Softw. 37.

Sen, S., Head, K.L., 1997. Controlled optimization of phases at an intersection. Transp. Sci. 31, 5–17.

Sethi, S.P., Thompson, G.L., 2000. Optimal Control Theory. Springer-Verlag, New York.

Wu, X., He, X., Yu, G., Harmandayan, A., Wang, Y., 2015. Energy-optimal speed control for electric vehicles on signalized arterials. IEEE Trans. Intell. Transp. Syst. 16, 2786–2796. http://dx.doi.org/10.1109/TITS.2015.2422778.

Yang, H., Jin, W.-L., 2014. A control theoretic formulation of green driving strategies based on inter-vehicle communications. Transp. Res. Part C: Emerg. Technol. 41, 48–60. http://dx.doi.org/10.1016/j.trc.2014.01.016.

Yeo, H., Skabardonis, A., Halkias, J., Colyar, J., Alexiadis, V., 2008. Oversaturated freeway flow algorithm for use in next generation simulation. Transp. Res. Rec. J. Transp. Res. Board 2088, 68–79. http://dx.doi.org/10.3141/2088-08.

Zhou, F., Li, X., Ma, J., 2017. Parsimonious shooting heuristic for trajectory design of connected automated traffic part I: theoretical analysis with generalized time geography. Transp. Res. Part B: Methodol. 95, 394–420. http://dx.doi.org/10.1016/j.trb.2016.05.007.

Zohdy, I.H., Rakha, H.A., 2014. Intersection management via vehicle connectivity: the intersection cooperative adaptive cruise control system concept. J. Intell. Transp. Syst. 1–16. http://dx.doi.org/10.1080/15472450.2014.889918.